Journal of Sound and Vibration 332 (2013) 6617–6636

Contents lists available at ScienceDirect

Journal of Sound and Vibration

journal homepage: www.elsevier.com/locate/jsvi

Review

Aeroacoustics research in Europe: The CEAS-ASC report on 2012 highlights

H. Bodén*, G. Efraimsson

Aeronautical and Vehicle Engineering, KTH, 10044 Stockholm, Sweden

ARTICLE INFO

Article history:
Received 22 May 2013
Accepted 1 July 2013
Handling Editor: P. Joseph
Available online 2 September 2013

ABSTRACT

The Council of European Aerospace Societies (CEAS) Aeroacoustics Specialists Committee (ASC) supports and promotes the interests of the scientific and industrial aeroacoustics community on an European scale and European aeronautics activities internationally. In this context, "aeroacoustics" encompasses all aerospace acoustics and related areas. Each year the committee highlights some of the research and development projects in Europe.

This paper is a report on highlights of aeroacoustics research in Europe in 2012, compiled from information provided to the ASC of the CEAS.

During 2012, a number of research programmes involving aeroacoustics were funded by the European Commission. Some of the highlights from these programmes are summarized in this paper, as well as highlights from other programmes funded by national programmes or by industry.

Enquiries concerning all contributions should be addressed to the authors who are given at the end of each subsection.

Contents

* Corresponding author. Tel.: +46 87908021.
E-mail address: hansbod@kth.se (H. Bodén).

0022-460X/$ - see front matter © 2013 Elsevier Ltd. All rights reserved.
http://dx.doi.org/10.1016/j.jsv.2013.07.002

1. Airframe noise

1.1. Reduction of trailing edge noise by gas injection

A prospective technique to reduce trailing-edge noise has been investigated by injecting gases at different densities [1]. As silencing fluid helium (a noble gas), carbon dioxide (a combustion product), and air were injected either into the boundary layer on the upper surface upstream of the trailing edge or at the trailing edge into the wake to understand the effect of the injection on the flow structure and the acoustic field. A computational approach based on large-eddy simulations (LES) and solutions of the acoustic perturbation equations was applied to trailing-edge noise of a flat plate at a free stream Mach number 0.6 and a Reynolds number of 12,000 based on the boundary-layer thickness at the inflow boundary. The results presented in Fig. 1 show that injection of additional momentum at the trailing edge changed the turbulent structures of the shear layer in which the Reynolds stress components were considerably decreased. The induced eddy motion prevented the abrupt change of the turbulence length scale, i.e., a smoother transition of the wall-bounded to the free-shear layer was observed. Furthermore, the two-point correlation evidenced that the flow injection diminished the sudden increase/decrease of the correlation length of convecting turbulence. The acoustic field of the upstream injection was louder than that of the trailing-edge injection. Regardless of the fluid density the trailing-edge injection showed the noticeable noise reduction. At the same mass flow rate the lightest gas (helium) of the trailing-edge injection decreased the acoustic power the largest.

Written by S.R. Koh: s.koh@aia.rwth-aachen.de, M. Meinke and W. Schröder, RWTH Aachen University, Germany.

1.2. Identification on Reynolds-number effects on slat noise

Slat noise measurements with small wind tunnel models like the DLR F16 (wing span 800 mm, retracted chord 300 mm) suffer from strong tonal peaks that mix up with broadband slat noise. In a joint effort in the mainframe of the German LuFo IV research program DLR, Airbus and EADS-IW designed a large scale high lift system (wing span 7200 mm, retracted chord 1200 mm) which was finally tested in the large low speed facility of DNW (DNW-LLF), see Fig. 2. The noise measurements in the open-jet of the DNW-LLF were conducted for wind speeds between 7 m/s and 65 m/s providing slat noise data in a Reynolds-

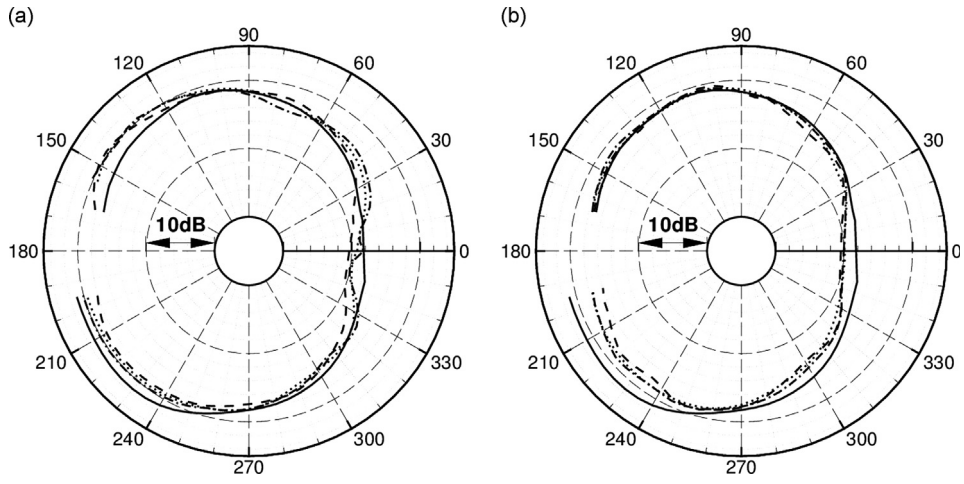

Fig. 1. Overall sound pressure level, solid line – no injection, dashed line – air injection, dotted line – helium injection, dotted line – carbon dioxide injection, at (a) upstream injection and (b) trailing-edge injection.

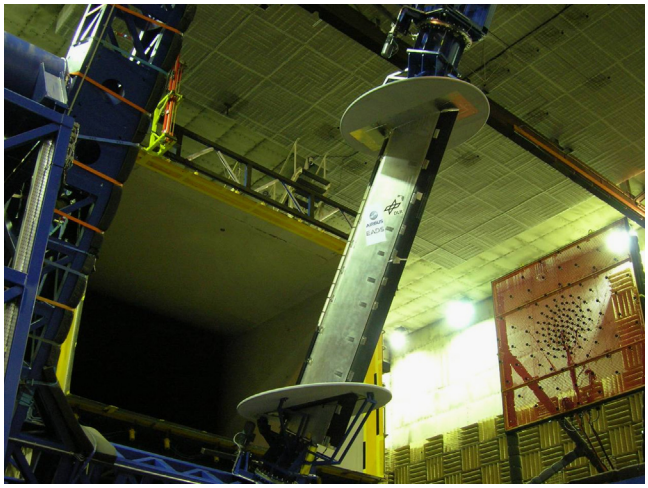

Fig. 2. Test setup of F15LS Test in DNW LLF.

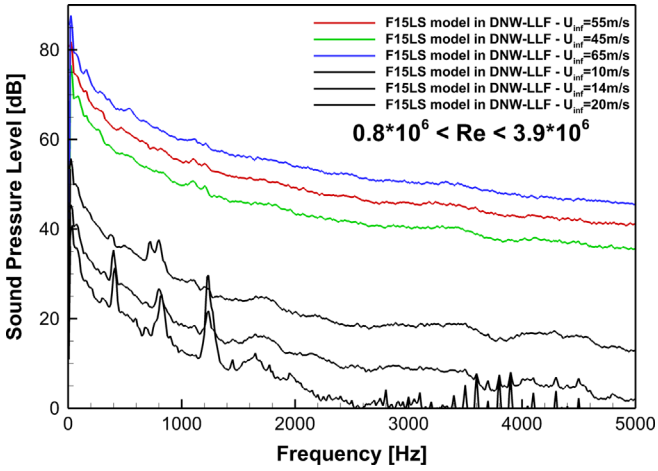

Fig. 3. Narrow band sound pressure level spectra as obtained for low and high Reynolds numbers. (For interpretation of the references to color in this figure legend, the reader is referred to the web version of this article.)

numbers range between 0.6×10^6 and 4.9×10^6. The lower Re-numbers relate to typical model scale tests at higher speeds as e.g. with DLR's F16 representing a 1/4 scale version of F15LS. It turned out that for high Reynolds numbers between 3.4×10^6 and 4.8×10^6 all acquired noise data showed no tones (Fig. 3, blue, green and red graphs). When simulating conditions as for the F16 in DLR's Acoustic Windtunnel Braunschweig AWB by reducing the wind speed tonal peaks showed up in the measured sound pressure level spectra (Fig. 3, black graphs). This first result of the tests gives evidence that low Reynolds number tests on high lift airfoils do not represent the broadband sound radiation typical for respective full scale components.

Written by M. Pott-Pollenske: michael.pott-pollenske@dlr.de, J. Delfs, DLR, Germany, A. Büscher, Airbus S.A., Germany, J. Reichenberger, EADS-IW, Germany.

2. Fan and jet noise

2.1. FLOCON: adaptive and passive flow control for fan broadband noise reduction – final results

The concept of the EU FP7, Call 1 collaborative research project FLOCON was to demonstrate methods capable of reducing fan broadband noise from aeroengines at source by 5 dB at approach and takeoff conditions, contributing to the European objective of reducing aircraft external noise per operation by 10 dB by 2020. To achieve this, the FLOCON consortium – consisting of 16 European partners – designed, manufactured and investigated experimentally and numerically noise reduction concepts and associated devices to reduce fan broadband noise from aero engines. The concepts were assessed by conducting lab-scale experiments to TRL 4 (Technology Readiness Level 4, validation at laboratory scale) and complemented by numerical simulations. The utilized state-of-the-art numerical methods were applied to design low broadband noise treatments and configurations and develop understanding of the mechanisms involved and extrapolate the results to a

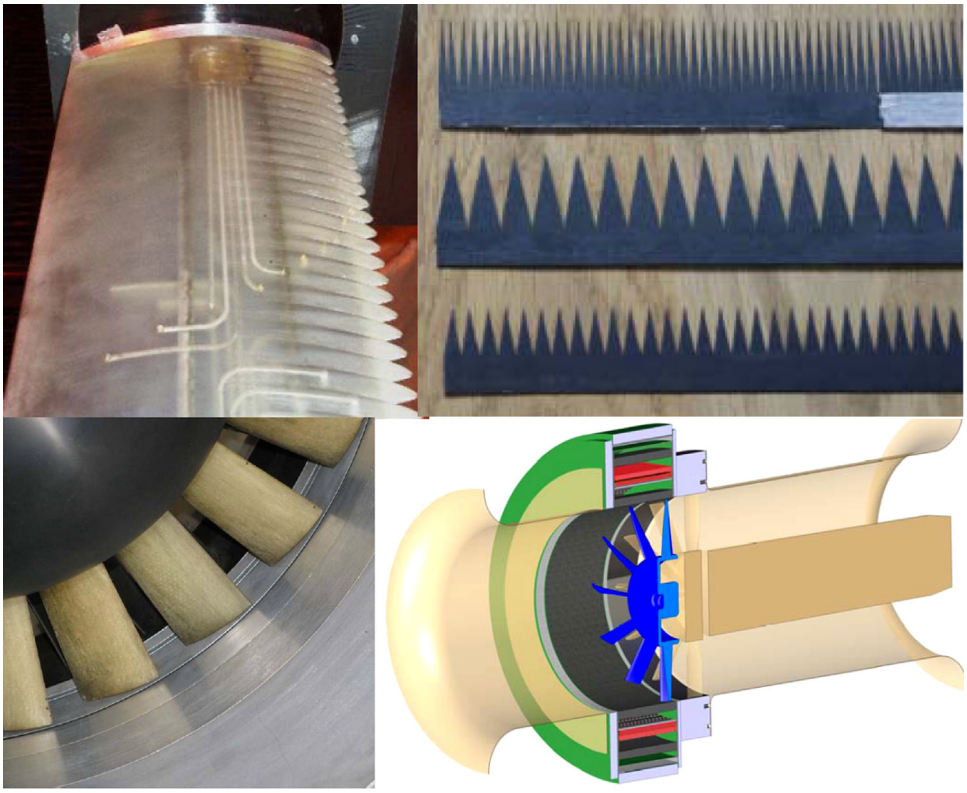

Fig. 4. Four turbomachinery broadband noise treatments investigated in FLOCON (from upper left to lower right): wavy leading edge, serrated trailing edge, inlet boundary layer suction, and special overtip absorber.

realistic aero engine environment, see Fig. 4. The best concepts were selected by balancing noise benefit and integration impact. The impact of scaling from lab- to engine-relevant operating conditions was assessed, as well as the side/complementary effect of broadband noise reduction features on fan tone noise. Furthermore, a comprehensive validation dataset has been created.

The broadband noise reduction concepts developed can be split into four different categories: The first category of concepts turned out to be successful in terms of experimental and numerical assessment as well as the extrapolation to a virtual aircraft platform and will be broadly applicable to fan stages of novel aero-engine designs. A second category of concepts were successful in terms of noise reduction potential, but need to be further analyzed in order to proof its applicability to a real engine design. A third category of methods was surprisingly low performing in the experimental application, although design as well as numerical results indicated a high broadband noise reduction potential. Finally, the fourth category of technologies simply turned out to not work as expected and should not be further investigated in the future.

FLOCON brought each concept of the mentioned categories 1–3 up to TRL4 (validation at laboratory scale). The technologies of the first category are recommended for the engine-ready level and an extrapolation to the expected performance at full engine scale was given. Others (from categories 2 and 3) need further evaluation to demonstrate their technical applicability and/or their noise reduction potential in other research projects.

An initial assessment of any penalties related to weight, aerodynamic performance, stress or mechanical complexity was performed with all deployed technologies. One category 1 technology, three category 2 technologies, and two category 3 technologies were finally identified and – at least the cat. 1 and 2 methods – need to be assessed in future European research projects to be applied in environments of higher TRL.

Written by L. Enghardt: lars.enghardt@dlr.de, German Aerospace Center (DLR), Berlin, Germany.

2.2. Investigation of the effects of initial disturbance level and Reynolds number in subsonic jets using large-eddy simulations

The effects of the initial conditions in isothermal round jets at a Mach number of 0.9 and diameter Reynolds numbers Re_D around 1e5 are investigated. For this, large-eddy simulations are performed using a low-dissipation low-dispersion finite difference scheme and relaxation filtering on a grid of 250 million points [2,3]. The influence of the initial conditions in jets is indeed known to be significant [4]. In experiments, however, several parameters are likely to vary simultaneously, resulting in difficulties to identify the impact of each one of them. In the simulations, the jets originate from a pipe in which a trip-like forcing is applied to the boundary layers in order to obtain, at the exit, the same mean velocity profile in all cases and a given value of peak turbulence intensities u'_{exit}/u_j. In a first study [5], the jets are all at Re_D=1e5, but display $u'_{\mathrm{exit}}/u_j = 0, 3, 6, 9$ or 12 percent. In a second study [6], on the contrary, the jets are at Re_D=2.5e4, 5e4, 1e5 or 2e5, but all exhibit $u'_{\mathrm{exit}}/u_j = 9$ percent. The effects of initial disturbance

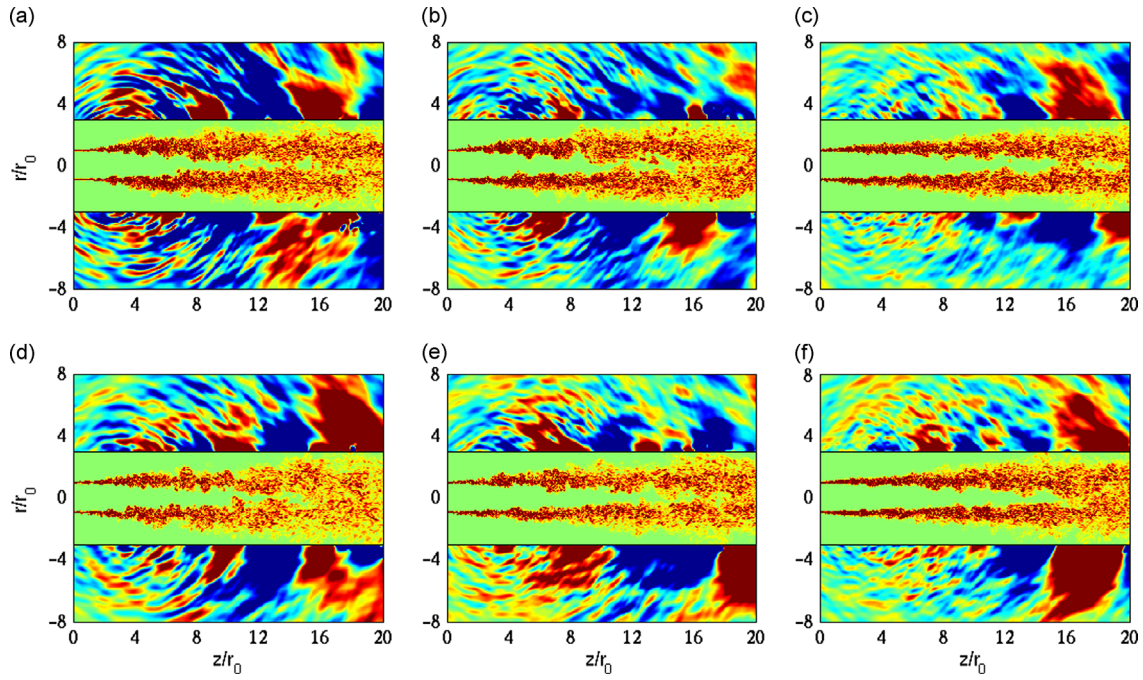

Fig. 5. Snapshots of vorticity and pressure, for jets at $Re_D=1e5$ with nozzle-exit peak turbulence intensities (a) $u'_{exit}/u_j=3$ percent, (b) 6 percent or (c) 12 percent, and for jets with $u'_{exit}/u_j=9$ percent at $Re_D=2.5e4$, (e) 5e4 or (f) 2e5.

level and Reynolds number are thus distinguished. With increasing u'_{exit}/u_j or Re_D, spectacular changes are observed in the jet flow and acoustic fields, including lower turbulence intensities, a longer potential core and weaker far-field noise. Snapshots of vorticity and pressure are represented in Fig. 5 to illustrate these trends.

Written by C. Bogey: christophe.bogey@ec-lyon.fr, Ecole Centrale de Lyon, Université de Lyon, France.

2.3. Near field pressure induced by compressible single-stream cold jets

Advanced signal processing methods based on wavelet transform have been applied to pressure data measured in the near field of a free jet at subsonic Mach numbers (up to 0.9) and for high Reynolds numbers (around 105). The wavelet technique allows for the separation of nearly Gaussian background fluctuations, interpreted as acoustic pressure, from intermittent pressure peaks induced by the hydrodynamic components. The method has been presented in [7] and successively extended to different Reynolds numbers in [8]. One of the main results achieved concern the spatial variation of the acoustic/hydrodynamic pressure field. It has been shown that the preferential radiation direction of the acoustic pressure is located at angles that, with respect to the flow axis, are larger than those of the hydrodynamic counterpart. The signature of the cone of silence has been evidenced as well and interpreted as the main directivity feature of the acoustic near field. Simultaneous velocity–pressure measurements permitted us to determine the flow regions exhibiting maximum correlation levels with the acoustic or hydrodynamic components of the pressure signals (Fig. 6). In the acoustic case, the largest correlations are determined at the end of the potential core. Conversely, the largest hydrodynamic pressure-velocity correlations are located close to the nozzle exit and in the far region, between $x/D=6$ and $x/D=9$, where turbulence is known to be strongly intermittent.

Written by R. Camussi: camussi@uniroma3.it, University Roma TRE, Italy, S. Grizzi:, Cnr – INSEAN, Italy.

2.4. "Buzz-saw" noise: prediction of the rotor-alone pressure field

"Buzz-saw" noise is generated by supersonic ducted fans. It is the dominant fan tone noise source from modern turbofan aircraft engines during take-off. The principal component of this noise source is due to the rotor-alone pressure field. At supersonic tip speeds this pressure field propagates upstream of the fan, and radiates noise from the turbofan intake. Prediction of this noise source involves nonlinear acoustics. Previous work by the authors has led to the development of a prediction scheme for buzz-saw noise generated by the rotor-alone pressure field. Previous validation of this prediction scheme was based entirely on reproducing the spectral characteristics of the noise source. In 2012, [9] published, for the first time, full validation of the buzz-saw noise prediction scheme by comparing measurement and prediction of the rotor-alone pressure field. The modeling is based on calculating the nonlinear propagation of a one-dimensional "N-wave" or sawtooth waveform as it propagates inside an intake duct. An example of the results, taken from [9], is shown in Fig. 7. This figure shows the rotor-alone pressure field and the EO frequency spectrum measured inside a rig-scale turbofan intake, as well as the simulated results. More examples of comparison of measurement with prediction are published in [9].

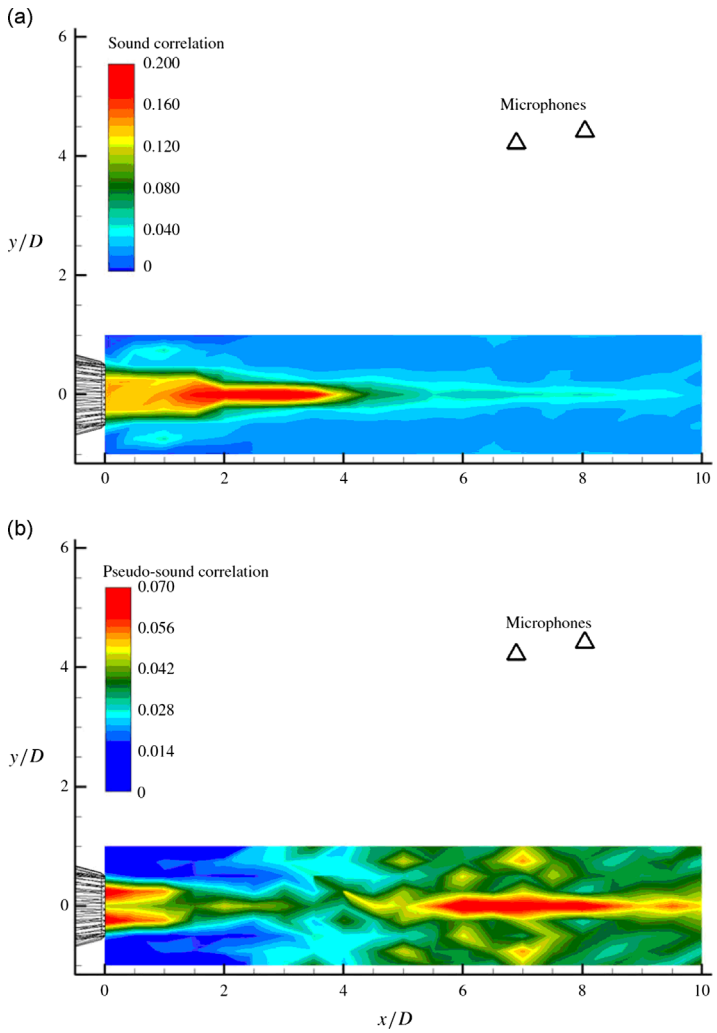

Fig. 6. Spatial distribution of the maximum amplitude of the cross-correlations between velocity and acoustic (a) and hydrodynamic (b) signals.

The work was funded by Rolls-Royce plc through the University Technology Centre in Gas Turbine Noise at the Institute of Sound and Vibration Research.

Written by A. McAlpine: am@isvr.soton.ac.uk, ISVR, University of Southampton, UK.

2.5. New insights on the incompleteness of duct modes in sheared flow

By deriving [10] the analytically exact Green's function for a mass point source in a cylindrical lined duct with uniform main flow and a linear-shear boundary layer (Fig. 8), a detailed analysis has been made of the role of the critical layer and other non-acoustic contributions associated with the boundary layer [10]. It was found that (1) the acoustic modes dominate the field unless they are all cut-off; (2) the critical layer contribution is only (relatively) small in combination with an associated non-acoustic mode; (3) for very thin boundary layers, the downstream field is dominated by the impedance wall-boundary layer instability (Fig. 9); (4) for relatively thick boundary layers the instability is nearly neutrally unstable; (5) if the mass source is positioned inside the boundary layer, vorticity is shed that may dominates the boundary layer field if the instability is not too strong (Fig. 10). The shown example is $\omega=10$, $m=5$, $M=0.5$, $Z=2-I$.

Written by S. Rienstra: s.w.rienstra@tue.nl, Eindhoven University of Technology, The Netherlands.

3. Helicopter noise

3.1. Effects of wind on the noise footprint of a helicopter

In order to minimize the noise footprint of a helicopter, DLR is working on the development of noise abatement flight procedures for helicopters. In a realistic environment, wind is almost always present and will affect the flight conditions of

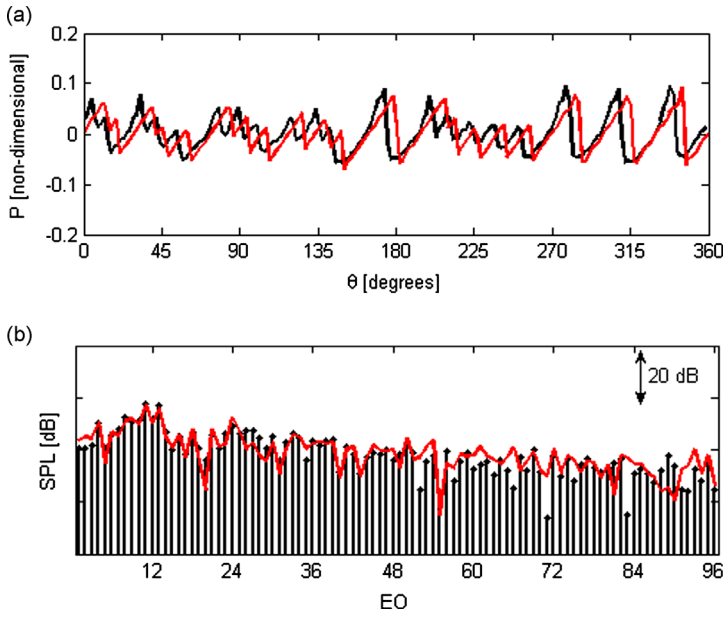

Fig. 7. (a) Example of comparison between measured (black) and predicted (red) rotor-alone pressure waveform for a hard-walled intake duct at fan speed 90 percent. (b) Example of comparison between measured (black) and predicted (red) EO frequency spectrum for a hard-walled intake duct at fan speed 90 percent. (For interpretation of the references to color in this figure legend, the reader is referred to the web version of this article.)

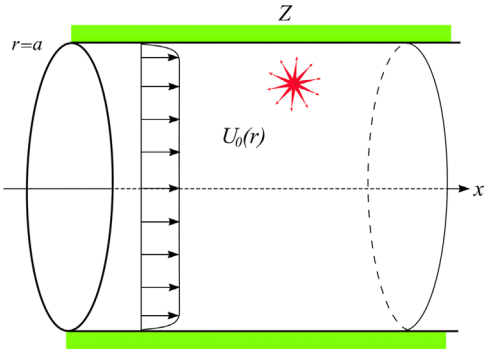

Fig. 8. Sketch of lined duct with non-uniform mean flow.

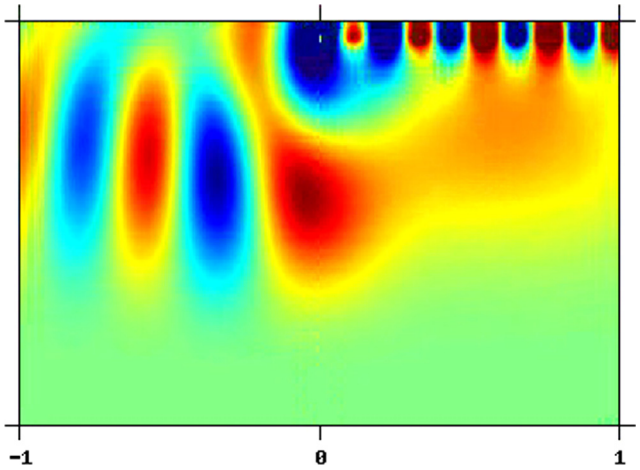

Fig. 9. Thin boundary layer (0.1 percent).

the helicopter and the propagation of sound through the atmosphere. To take the effects of wind, wind gradients and temperature gradients into account the computational method (SELENE) is extended with a ray tracing algorithm [11]. With this extension the influence of wind on the Sound Exposure Level (SEL) noise footprint can be investigated. This also allows to separately assess changes due to different flight conditions and changes due to different sound propagation.

Figs. 11–14 show the computed noise footprints of a reference procedure, the difference between contours is 5 dB(A). The flight direction is from left to right and indicated by the dashed black line. The wind direction (Figs. 12–14) is from right to left. Fig. 11 shows the case of no wind. In Fig. 12 only the influence of wind on the propagation of sound is taken into account, while in Fig. 13 only the influence of wind on the flight conditions is considered. Fig. 14 corresponds to the real world situation where the influence of wind on both the flight conditions and on the propagation of sound is taken into account.

In general it can be concluded that contours directly below the flight path are dominated by changes in flight conditions, while contours further away are dominated by propagation effects.

Written by W.F.J. Olsman: jurrien.olsman@dlr.de, DLR, Institute of Aerodynamics and Flow Technology, Germany.

3.2. *Efficient formulations for rotorcraft aeroacoustics*

A novel frequency-domain formulation for the prediction of the tonal noise disturbance induced by rotating blade systems in arbitrary steady motion has been presented in [12]. It is derived from the time-domain Farassat 1A boundary integral formulation and represents thickness and loading noise as harmonic responses to body kinematics and aerodynamic loads. The proposed frequency-domain solver is applicable to those configurations where tonal noise is

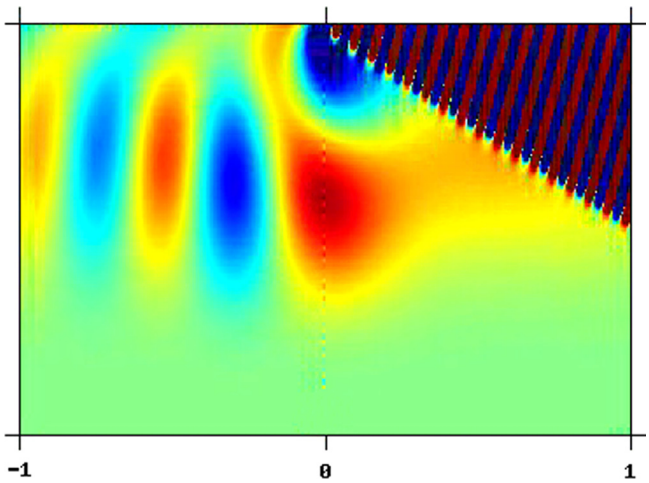

Fig. 10. Thick boundary layer (5 percent), source inside boundary layer.

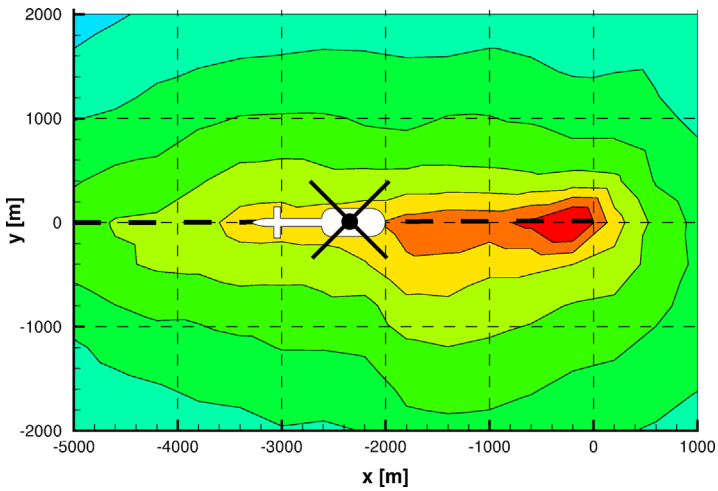

Fig. 11. SEL noise footprint in case of no wind.

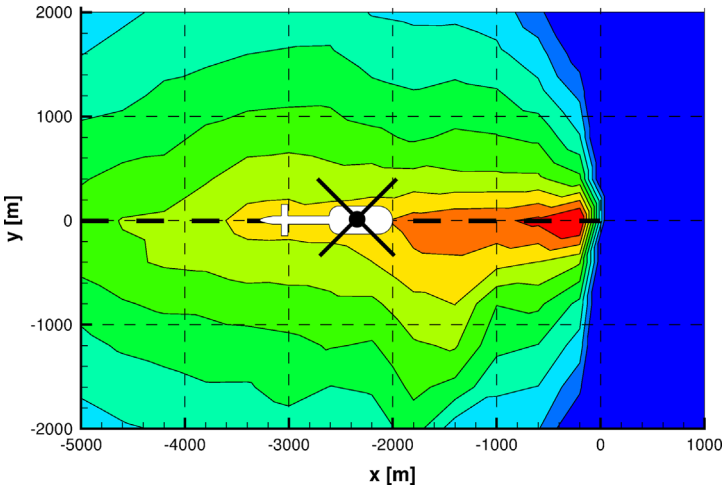

Fig. 12. SEL noise footprint in case of head wind. Influence of wind on propagation of sound only. The appearance of a shadow zone, due to refraction, can be seen on the right.

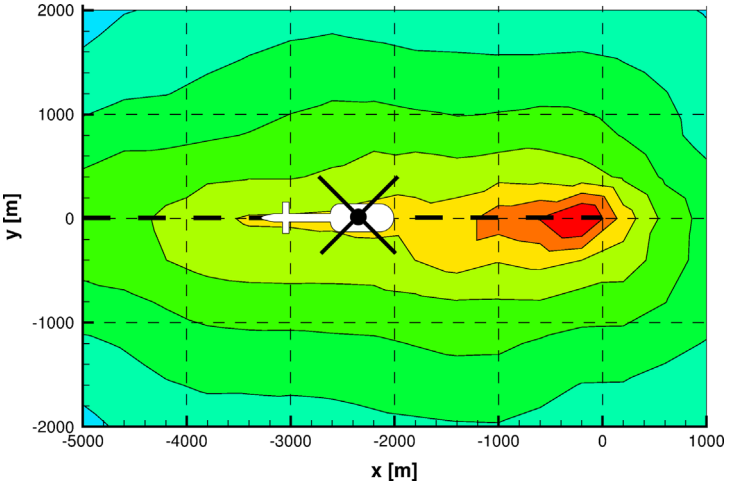

Fig. 13. SEL noise footprint in the case of head wind. Influence of wind on flight conditions only.

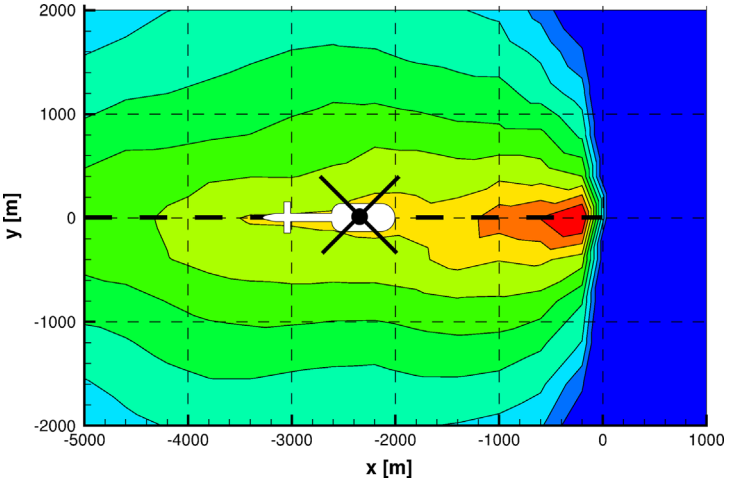

Fig. 14. SEL noise footprint for the case of head wind. Influence of wind on both flight conditions and propagation of sound has been taken into account. On the right a shadow zone is seen.

dominant. It has been proven that the availability of the aeroacoustics transfer matrices (relating blade airloads/normalwash to noise spectra) is useful for a detailed analysis of the mechanism of sound emission and the determination of the more strongly radiating noise sources. This formulation is suited to be integrated within an analytical-numerical aerodynamic/aeroacoustic formulation, developed by the authors, for the analysis of configurations dominated by local high frequency changes (both in time and space) of blade inflow velocity [13]. Specifically, the Farassat 1A formulation is combined with the frequency domain Küssner–Schwarz formulation for the sectional, unsteady aerodynamic loads, starting from the knowledge of the downwash on the airfoil. The blade inflow due to wakes is assumed to be evaluated through a 3D, unsteady, panel method formulation suited for the analysis of rotors operating in a complex aerodynamic environment. This aerodynamic/aeroacoustic model gives a computationally efficient solution procedure that may be conveniently applied in preliminary design/multidisciplinary optimization applications. It has been validated against the acoustic field obtained through the time-marching panel-method solver.

Written by M. Gennaretti: m.gennaretti@uniroma3.it, G. Bernardini, University ROMA TRE, Italy, C. Testa, CNR-INSEAN Italy.

4. Propeller noise

4.1. Aerodynamic and acoustic optimization of a contra- rotating open rotor with experimental verification

The present study [14–16] demonstrates an aerodynamic and acoustic optimization methodology of a contra-rotating open rotor (CROR). The main challenge of the design effort undertaken was to improve the overall propulsive efficiency at *top of climb* operating conditions while at the same time improving the acoustic characteristics at *take-off* or *sideline* conditions respectively. Apart from these global objectives, a number of constraints such as fulfilling thrust requirements at various flight regimes as well as basic mechanical criteria such as stress limitations to ensure a safe operation needed to be respected and pose additional challenges for the design effort. Both the aerodynamic and acoustic characteristics of several typical CROR configurations as shown in Fig. 15 were studied by means of a coupled CFD/FW-H approach and corresponding experiments conducted in TsAGI WT104 wind tunnel. Although the design efforts were undertaken neglecting the installation of the open rotor to the aircraft, the experimental results representing the sum of sound pressure level of the interaction harmonics as given in Fig. 16 confirm the success of the numerical optimization effort for configuration V2.0. In comparing with the reference configuration V1.1, an average acoustic benefit of 3.2 dB was measured at sideline conditions for the optimized version V2.0. The main driver of the acoustic improvement was mainly in terms of a reduction of the wake velocity deficit of the V1.1 front rotor. The wake strength reduction led to a decrease of the sum of the interaction tones over the entire directivity.

Written by R. Schnell: rainer.schnell@dlr.de, J. Yin, S. Funke and H. Siller, German Aerospace Center (DLR), Germany.

5. Techniques and methods in aeroacoustics

5.1. De-reverberation of closed-section wind tunnel noise measurements by conventional beamforming

The performance of conventional beamforming and deconvolution techniques to provide de-reverberated noise source spectra from microphone array measurements in hard-walled closed-test-section wind tunnels has been assessed [17]. By interpreting de-reverberation as the ability to separate real acoustic sources within the test section and their image sources outside, the de-reverberation performance relies on the spatial resolving power of beamforming. Following classical beamforming resolution criteria, two experimental campaigns have been conducted, one being a priori favorable for de-reverberation and the other one being a priori unfavorable. The favorable test campaign has been performed in Onera's F1 facility (Fig. 17). The noise source is a streamlined electro-acoustic source at a significant distance from the walls. Microphone array measurements have been analyzed by beamforming and the acoustic spectrum generated by the

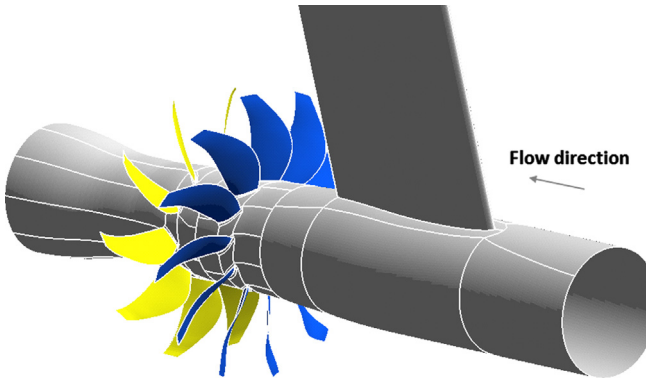

Fig. 15. Schematic of the simulated CROR geometry with the structural pylon.

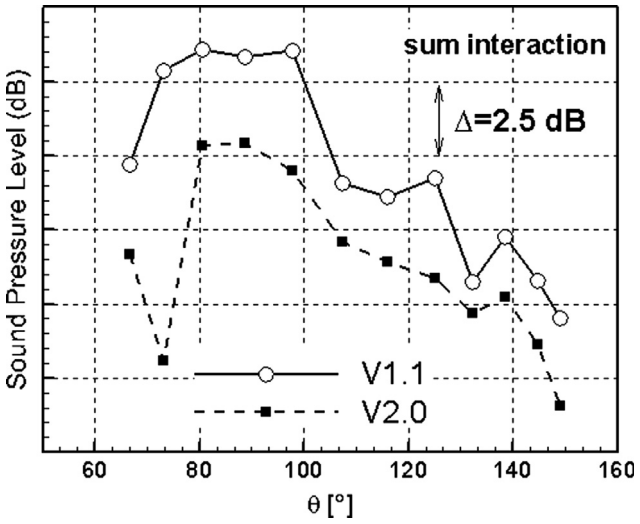

Fig. 16. Experimental verification on the reduction of the sum of the interaction harmonics for the optimized CROR Version V2.0.

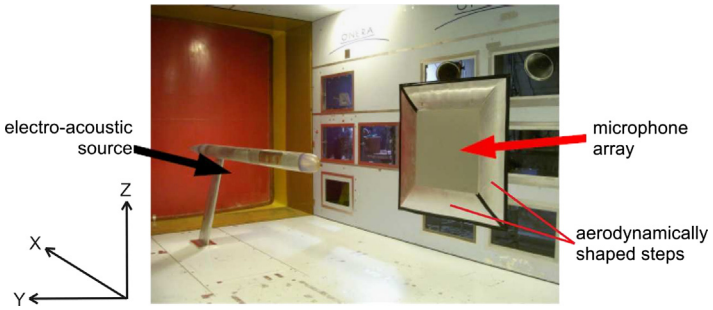

Fig. 17. Streamlined electro-acoustic source in F1.

electro-acoustic source has been obtained by de-convolution. A fair agreement with reference free-field measurements in the Onera Cepra19 anechoic wind tunnel was noticed, which validates de-reverberation, as expected. The un-favorable test campaign has been carried-out in the Onera F2 facility. A loudspeaker close to the wall has been used and microphone array data have been analyzed following a similar procedure as in F1. In this case however the loudspeaker and its virtual image source due to acoustic reflexion are not separated by beamforming at low-frequencies. Consequently, the free-field acoustic spectrum generated by the loudspeaker cannot be estimated, as expected. This work therefore shows that closed-section wind tunnel noise measurements can be de-reverberated by beamforming and that the validity of beamforming regarding reverberation issues can be predicted. To perform reliable beamforming noise measurements, additional requirements should however be satisfied too, such as efficient data de-noising, low directivity effects etc.

Written by V. Fleury: vincent.fleury@onera.fr, and R. Davy, Onera, France.

5.2. Nearfield acoustic holography in wind tunnel with LDV measurements

With the increased interest in transport noise research, aeroacoustic source localization on models in wind tunnels is a relevant issue today. For a long time, beamforming, based on farfield microphone measurements, has been the reference method. Similar to in free field conditions, an extension of Nearfield Acoustic Holography to aeroacoustic source characterization in uniform subsonic flows can be a complementary method to beamforming. Onera [18–20] has developed this type of method from non-intrusive optical measurements, using the convective Kirchhoff–Helmholtz integral formula and real-space convective propagators built on the convective Green's function. The approach is especially focused on the convective velocity-to-pressure propagators allowing the reconstruction of acoustic fields towards the source plane in order to apply NAH for hologram laser measurements which provide acoustic and aerodynamic velocities. Numerical studies show that this method is relevant in the case of classical aeroacoustic sources (i.e. monopoles or dipole sources, as in Fig. 18) radiating at various subsonic Mach numbers (up to $M=0.75$) and frequencies (1–5 kHz). The reconstructed acoustic fields allow a good localization and quantification of maximal pressure magnitude (error <2 dB) without any additional inverse method or hypothesis about the sources. In order to confirm the efficiency of this method, experiments have also been performed in a laboratory wind tunnel ($M=0.21$) with a flush-mounted loudspeaker simulating a monopole source (2 kHz).

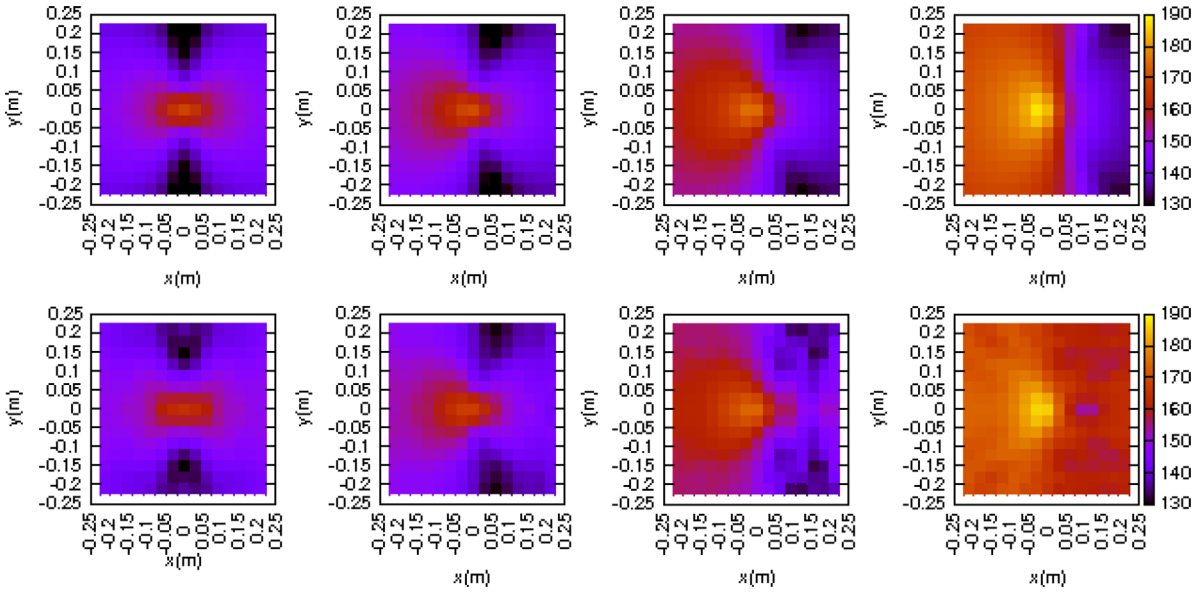

Fig. 18. Reconstructed acoustic pressure level in source plane obtained by the theory of dipole sources (top) and NAH (bottom) for $M=[0;0.25;0.5;0.75]$, $f=2$ kHz, distance sources-Hologram plane $=5$ cm.

Laser Doppler Velocimetry (LDV) was used to obtain nearfield measurements of normal fluctuation velocity components without disturbances created by flow-microphone array interaction.

Written by H. Parisot-Dupuis: helene.parisot dupuis@onera.fr, F. Simon, E. Piot and F. Micheli, Onera, France.

5.3. Time-reversal technique to localize acoustic sources in a wind-tunnel flow

The possibility of using the time-reversal technique to localize acoustic sources in a wind-tunnel flow has been investigated [21]. While the technique is widespread, it has scarcely been used in aeroacoustics up to now. The proposed method consists of two steps: in a first experimental step, the acoustic pressure fluctuations are recorded over an array of microphones, and the mean flow profile is measured; in a second numerical step, the experimental data are time-reversed and used as input data for a numerical code solving the linearized Euler equations (Fig. 19). The simulation achieves the back-propagation of the waves from the array to the source and takes into account the effect of the mean flow on sound propagation, provided that the mean flow direction is reversed. From the time-reversed simulation, it is then possible to calculate a distribution of the square pressure, leading to an imaging of the source similar to beamforming results, and making possible the aeroacoustic source localization.

A generic experiment has been set up with a well-controlled acoustic monopole sound source embedded in a flat plate, in a wind-tunnel flow at Mach number 0.11 bounded by the flat plate on its bottom side.

The source localization is obtained with an error of less than a wavelength, for harmonic and wide-band sound sources (Fig. 20). The possibility of localizing a dipole sound source has also been demonstrated. The advantage of a time-reversal based method over the classical beamforming method is its flexibility, enabling to take accurately into account arbitrary mean flow profiles, and possibly an-isothermal propagation medium, such as for heated jets for instance.

Written by T. Padois: vincent.valeau@univ-poiters.fr, C. Prax, V. Valeau and D. Marx, Institut Pprime, Poitiers, France.

5.4. Impedance eduction technique based on LDV fields above aircraft liners

Reduction of noise generated by aircraft turbofans can be achieved by lining the nacelle with acoustic treatments, typically made of honeycomb topped by a perforated sheet. Optimization of these liners requires an accurate knowledge of their absorbing properties in presence of a grazing flow. These properties are represented by the acoustic impedance, generally measured directly, for instance with the in-situ method, or extracted thanks to an eduction technique, which relies on matching between numerical simulations and acoustic measurements. Usually, objective functions of eduction techniques are based on wall acoustic pressure measurement. The new eduction procedure developed by Onera [22,23] is based on acoustic Laser Doppler Velocimetry measurements (Fig. 21) and Discontinuous Galerkin (DG) simulations. The experimental approach has the advantage of being non-intrusive and offers the possibility to build objective functions formulated on two-dimensional velocity fields. Moreover, the sheared velocity profile of the duct flow can be measured as well. Numerical simulations solve the harmonic Linearized Euler Equations using discontinuous finite elements. Such a DG formulation is particularly well-suited to solving aero-acoustics problems, even for complex geometries or discontinuous

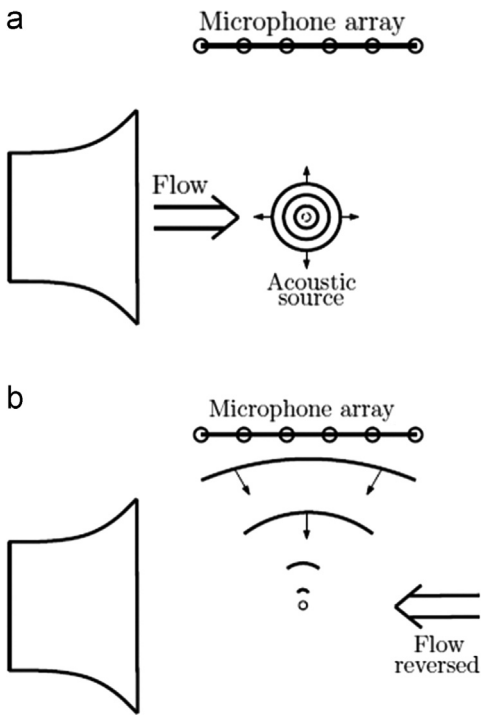

Fig. 19. Principle of the time-reversal based method for localizing experimentally a sound source in a flow. (a) Experimental measurement and (b) time-reversed simulation.

boundary conditions (i.e. liner partitioning). The opportunity to displace the observation region towards the lining sample should contribute to get impedances more representative of the actual behavior of the liner. The propagation model and the eduction process have been successfully validated using NASA benchmark data (Fig. 22).

Written by J. Primus: julien.primus@onera.fr, E. Piot and F. Simon, Onera, France.

5.5. Intrinsically optimized finite differences schemes for computational aeroacoustics

As a part of the effort towards the development of advanced computational means for the aircraft noise prediction, ONERA has promoted the development of Computational Aeroacoustics (CAA) tools, such as the time-domain / finite differences solver *sAbrinA.v0* [24–26]. Several advances were recently achieved in the framework of a PhD thesis [24] where a new class of finite difference (FD) propagation schemes was developed. These so-called *intrinsically optimized* FD schemes [27,28] are of optimal accuracy, thanks to an optimization process that is based on a minimization of the scheme's leading-order truncation error, rather than on an optimization of the scheme spectral properties [29,30]. The intrinsically optimized FD schemes enable the use of coarser grids compared to other FD schemes. As an example, with no more than 4 points per wavelength (PPW), an intrinsically optimized FD scheme of 15 points guarantees that the error of the group velocity is less than 0.1 percent. Compared to the accuracy of a classical 7-points/6th order standard FD scheme (which corresponding minimal PPW is 12), this represents a gain of 3 per direction, i.e. a factor 27 in 3D. The intrinsically optimized FD schemes were validated in academic test cases of increasing complexity [27,28] (see Fig. 23), before they were successfully applied to a realistic problem, given by the noise emission of a simplified nose landing gear in an approach flight. Relying on a weakly coupled CFD-CAA calculation [31], this case allowed to further validate the intrinsically optimized FD schemes, as well as to illustrate their potentialities (Figs. 24–27).

Written by G. Cunha; gcoelhocunha@gmail.com, S. Redonnet, ONERA, France.

5.6. Scattered field predictions of the broadband noise generated by a low-speed axial fan

The aeroacoustic activities carried out at the von Karman Institute for Fluid Dynamics (VKI) have recently addressed numerical investigation of the broadband noise emitted by low-speed cooling fans. An innovative approach has been developed within the FP7 EC project ECOQUEST ("Efficient Cooling systems for Quieter Surface Transport", Grant Agreement no 233541) for the prediction of the scattering of broadband noise emitted by steady and rotating airfoils. The method is based on Amiet's theory, extended to provide the incident acoustic velocity power spectrum, and the Acoustic Transfer Vector (ATV) technology implemented in the Boundary Element solver of the Virtual.Lab Acoustics solver. It has been validated for

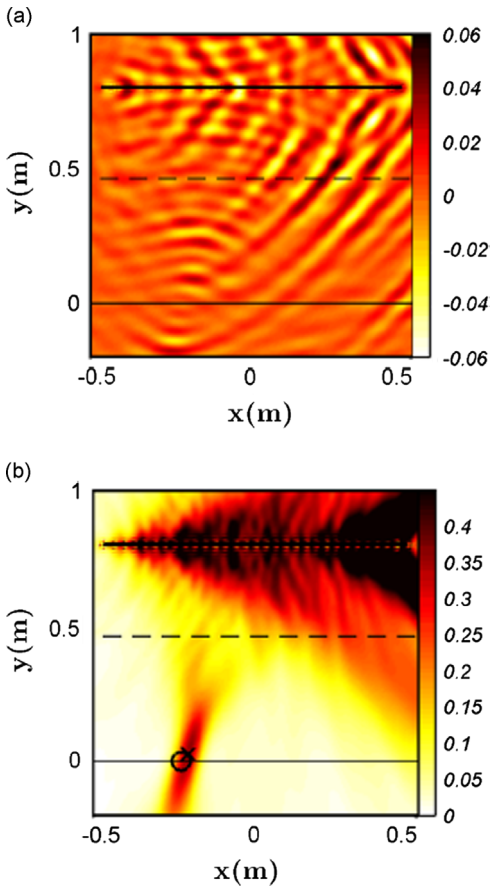

Fig. 20. (a) Pressure snapshot of the simulated time-reversed field for a wide-band experimental sound source in a wind-tunnel flow (Mach number 0.11). The sound source is at (−0.25, 0). (b) Square pressure distribution in the range 2500–5500 Hz [21]. The circle and cross symbols indicates the known source position and its estimation. The thick plain line, dashed line and plain line indicate respectively the array, the shear layer and the flow lower boundary.

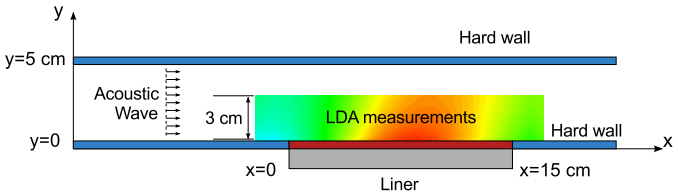

Fig. 21. 2D scheme of the test section of the Onera bench (B2A) in the grazing acoustic incidence configuration.

the case of a steady NACA0012 airfoil placed in the transition part of a turbulent jet, with a scattering screen located in the propagation region [32], and for the sound emitted by a low-speed rotating fan, also scattered by a flat screen [33].

Written by C. Schram: christophe.schram@vki.ac.be, von Karman Institute for Fluid Dynamics, Belgium.

6. Aircraft interior noise

6.1. Cabin noise source ranking based on A320 flight test data

Flight tests on DLR's A320–232 research aircraft "D-ATRA" were conducted within the German national (LuFo IV) project SIMKAB [34,35] to improve present cabin noise prediction methods through identification of the relevant noise sources and their respective transfer paths into the cabin. Extensive measurement data were collected using surface pressure microphones at the fuselage, acceleration sensors at various positions within the fuselage structure and microphones installed in the cabin interior. Test parameters included various flight speeds, flight altitudes, as well as different engine and air conditioning settings. The parametric approach allowed isolating the noise impact as attributed to the turbulent boundary layer (TBL) on the fuselage, engine jet noise or the air conditioning system (ACS), see Fig. 25 [36,37].

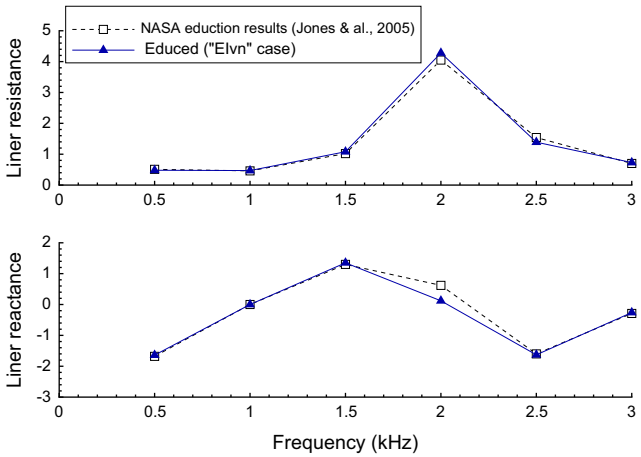

Fig. 22. Liner impedance educed from simulated velocity ("Elvn" case) on the NASA GIT.

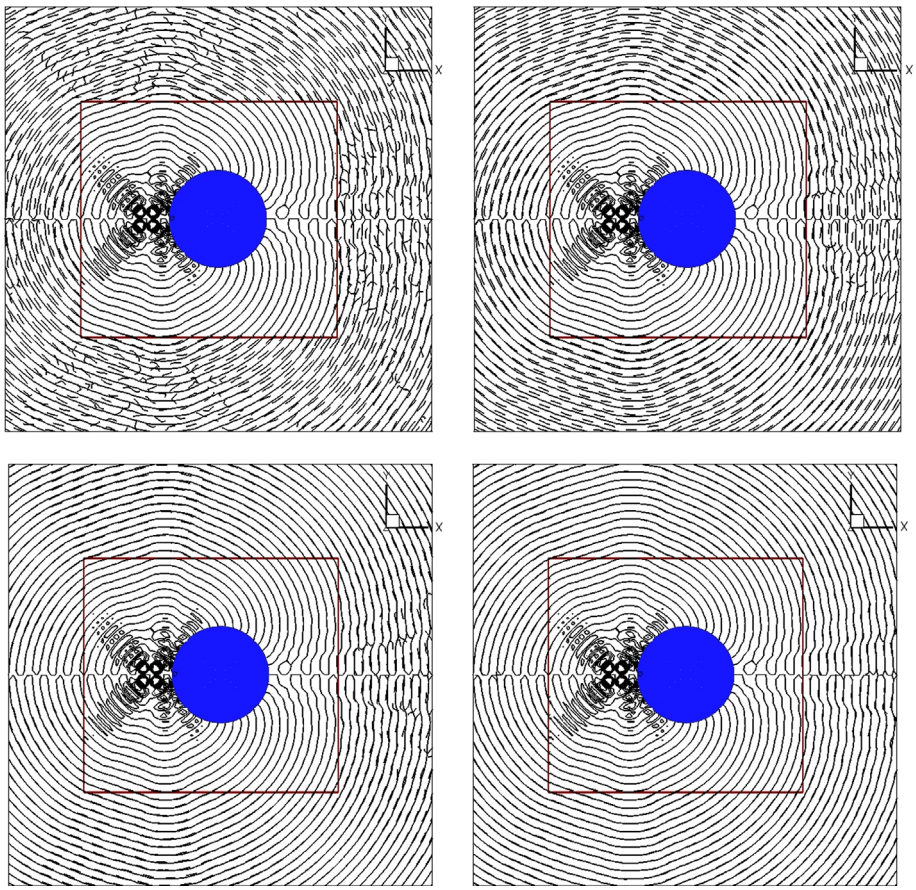

Fig. 23. Scattering by a 3D sphere of a high frequency (kR=6□) acoustic quadrupole in an infinite medium at rest. CAA calculations conducted with the sabrinA.v0 code[1] on a very coarse Cartesian grid (3.3 PPW), with the help of various FD space derivatives: standard FD schemes of 7 (top/left) or 11 (top/right) points, and intrinsically optimized FD schemes of 11 (bottom/left) or 15 (bottom/right) points. Validation by comparison of numerical outputs (in dashes, out of the red box) with analytical data (in line, within the entire domain). (For interpretation of the references to color in this figure legend, the reader is referred to the web version of this article.)

The latter revealed that cabin noise contributions originating from both TBL excitation and jet noise increase towards the rear of the fuselage, reflecting the natural growth of the TBL thickness and typical jet noise radiation characteristics. Contrary to that the ACS contributions, mainly caused by the mixing unit located underneath the cabin floor in the central area of the fuselage, are of minor importance. Overall sound pressure levels in the cabin rise significantly with increasing flight speed while the relative importance of the jet noise contribution increases. TBL-contributions grow with ambient

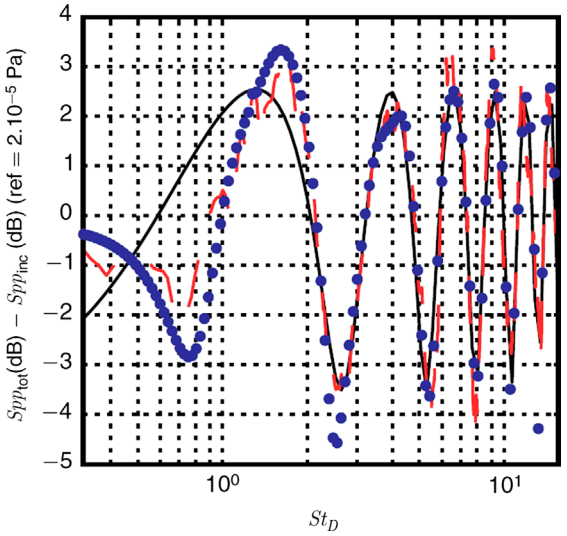

Fig. 24. Scattered component of the acoustic field radiated by the jet-airfoil interaction in presence of a reflecting screen in the propagation region, St_D based on the jet outlet velocity and airfoil chord. Dashed line: experiments, solid line: simplified image-source model, symbols: Amiet-ATV model.

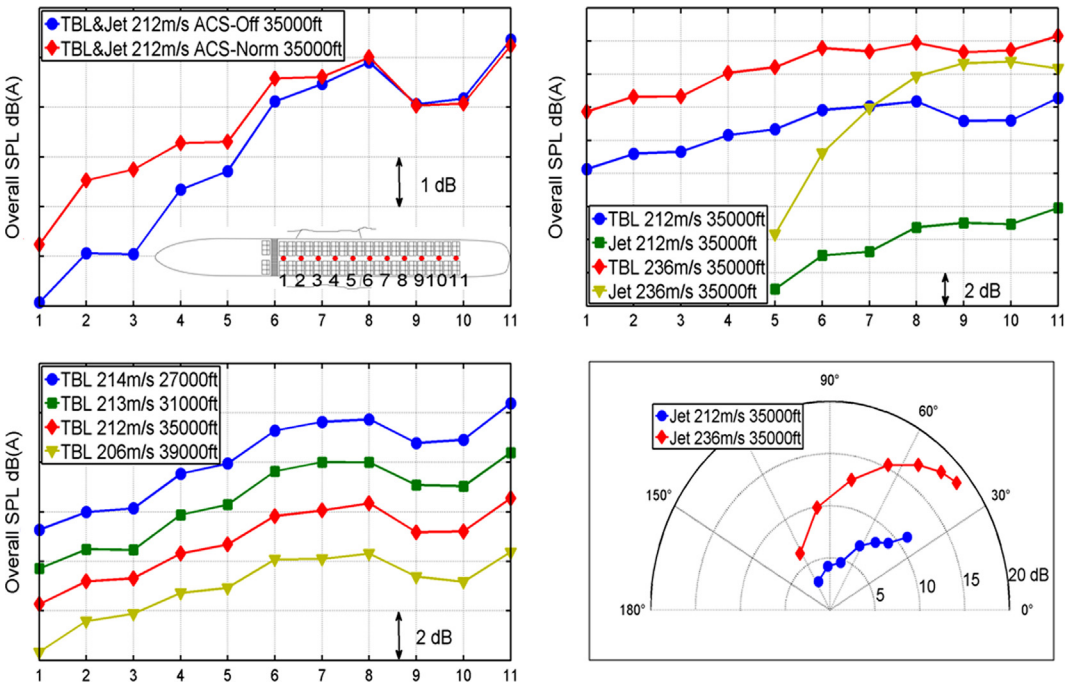

Fig. 25. Longitudinal distribution of the A-weighted overall sound pressure levels in the cabin for different operating conditions of the air conditioning system at cruise (upper left). Extracted TBL and jet noise contributions for different flight speeds at cruise (upper right). Extracted TBL contributions for different flight levels (lower left). Resulting jet noise directivity for "D-ATRA"'s AE V2500 engine after passage of the noise through the fuselage structure (derived from interior microphone measurements for emission time of sound, lower right).

density (decreasing altitude). During cruise at higher Mach number (236 m/s, 35000 ft) interior noise at the rear due to the TBL and to jet noise are of similar magnitude. Frequency and velocity dependent transfer functions between the fuselage excitation and interior noise were derived.

Written by N. Hu: nan.hu@dlr.de, H. Buchholz, M. Herr, C. Spehr and S. Haxter, DLR, Germany.

6.2. Scaling laws for the elastic panel TBL interaction

Different scaling laws are derived to find out a dimensionless representation of the frequency response for a thin elastic panel excited by a stationary turbulent boundary layer [38]. These laws are obtained using both a conventional dimensional

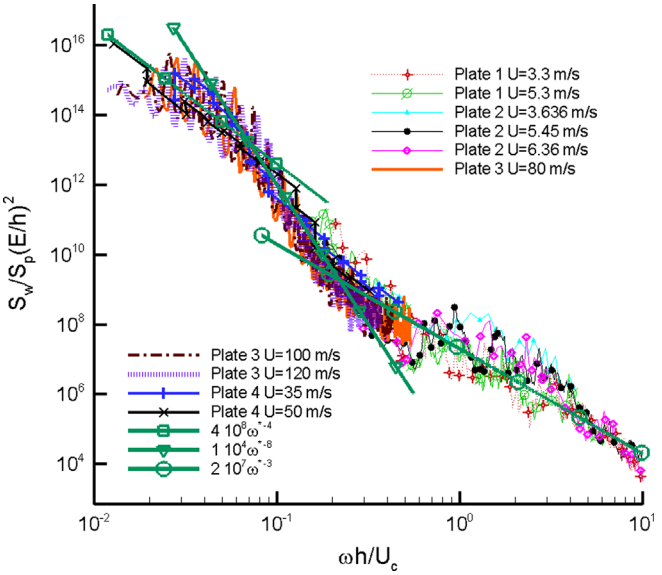

Fig. 26. Dimensionless plate displacements. Scaling laws are obtained by dimensional analysis.

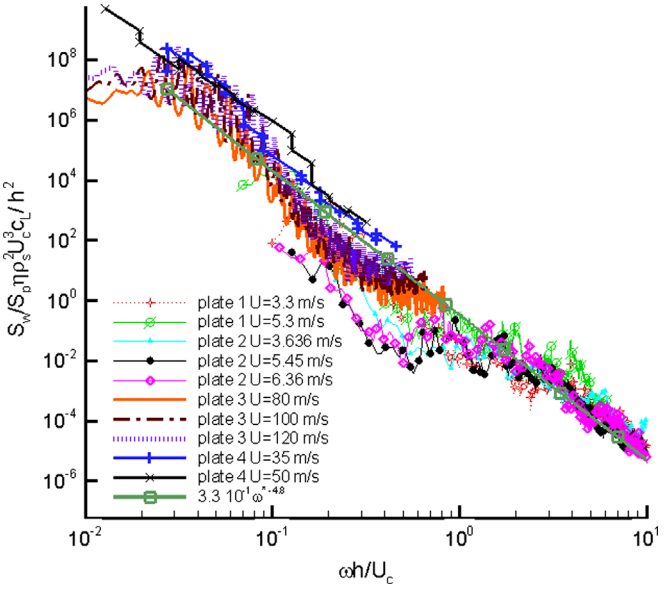

Fig. 27. Dimensionless plate displacements. Scaling laws are obtained by energy formulation.

analysis and an energy response formulation. They contain the most significant structural and fluid-dynamic parameters involved in the phenomenon. The proposed dimensionless groups are used for representing a quite large amount of experimental data concerning the response of four types of plates of different size and material, in air and in water flow, excited by turbulent boundary layers. Within these data sets, it is shown that all the presented experimental measurements collapse very close one to each other. Simple analytical expressions for the dimensionless curves are obtained that can be used to perform fast preliminary predictive steps. In fact, it is shown that an estimate of the power spectral densities of the displacement response in the whole frequency range can be obtained, starting from the desired test conditions i.e. material properties, geometrical characteristics and flow velocities, from the knowledge of the boundary layer thickness and of the friction velocity necessary to define the pressure power spectral density. At present time, the effectiveness of the proposed dimensionless forms has been demonstrated for thin plates only and an extension to more complicated structural components is needed.

Written by S. De Rosa: e.ciappi@insean.it, F. Franco, Università degli Studi di Napoli "Federico II and E. Ciappi, CNR-INSEAN, Italy.

6.3. Wall pressure fluctuations induced by supersonic turbulent boundary layers

Reduced levels of internal and external panel vibrations of an aerospace vehicle are desired to avoid fatigue problems and structural damages. In order to determine the vibro-acoustic behavior, detailed statistics of wall-pressure fluctuations (WPF) in the high-speed regime are required. Most of the investigations devoted to the analysis of the WPF made in the past years were carried out in incompressible flow conditions. The literature shows that pressure spectra modeling in supersonic conditions is rather incomplete since our knowledge of the multi-variate statistics of the wall pressure fluctuations induced by equilibrium supersonic boundary layers, is quite limited and needs to be improved. In a recent paper [39] the authors analyzed a DNS database providing wall pressure fluctuations over a flat plate without pressure gradients, at Mach numbers ranging from 2 to 4 and over a relatively extended range of moderate Reynolds numbers. The analysis was mainly targeted towards the accurate characterization of the wall pressure coherence function and the capability of existing theoretical models to predict the statistics has been investigated and discussed as well (Fig. 28). The results achieved suggest that the main statistical properties of the WPF induced by supersonic boundary layers is similar to that commonly observed in incompressible flow conditions and that standard models, such as the Corcos' and Efimtzov's ones, can be used at high Mach numbers, provided the empirical coefficients are properly adjusted.

Written by A. Di Marco, R. Camussi, University Roma TRE, Italy, M. Bernardini and S. Pirozzoli University "La Sapienza", Italy.

7. Miscellaneous topics

7.1. A novel thrust reverse noise detection tool for airports

Many airports all over the world have established some kind of restrictions for the use of thrust reverse, especially during the night period, as a way of reducing the noise impact and number of complaints in the vicinity of airports. This is the case of Madrid airport, where Universidad Politécnica de Madrid, in collaboration with AENA, SEA Milano, and Politecnico di Milano have been researching, and developing new techniques to improve the detection and classification of thrust reverse noise among other noise sources present in the airport. Based in a traditional approach, the thrust reverse noise detection (TREND) tool detects two consecutive sound events, and applies pattern recognition techniques for the classification of each of them as landing and thrust reverse. A second improvement refers to the use of a microphone array, which enables tracking the direction of the arrival of the sound, thus improving the classification rates. By taking the latter, it is also possible to track the location of the aircraft along the runway, which enables sound pressure measurements to be transformed into sound power level estimations, thereby enhancing events and improving their detection. Although TREND must be optimized and customized, the results have shown quite good classification rates (90 percent). Detailed information of the proposed TREND system can be found in [40,41].

Written by C. Asensio:casensio@i2a2.upm.es, Universidad Politécnica de Madrid, Spain.

7.2. On the power spectra of sound transmitted through turbulence

The power spectrum of sound received from a known acoustic source after transmission through a region of turbulence is calculated by a convolution with a distortion function [42]. The latter specifies the modification of the acoustic power spectrum as it propagates through the turbulent region. The distortion function is the Fourier transform with regard to time of the characteristic function of a bivariate aleatory process, whose random variables are the acoustic phase shifts of two neighboring waves. The phase shifts are due to the Doppler effect of the random turbulence velocity and are a function of position and time. The turbulence spectrum is used to calculate the rms phase shift and also the correlation time in the correlation coefficient. This specifies the received power spectrum for any type of source, viz. a monochromatic or tonal

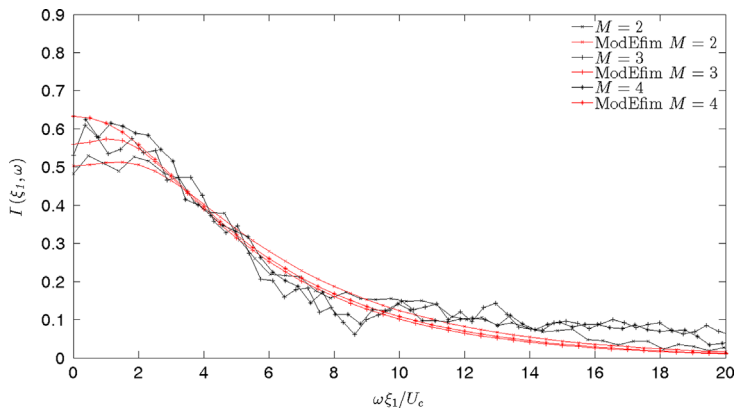

Fig. 28. Efimtsov modelization of the streamwise coherence as a function of the normalized frequency for different Mach numbers.

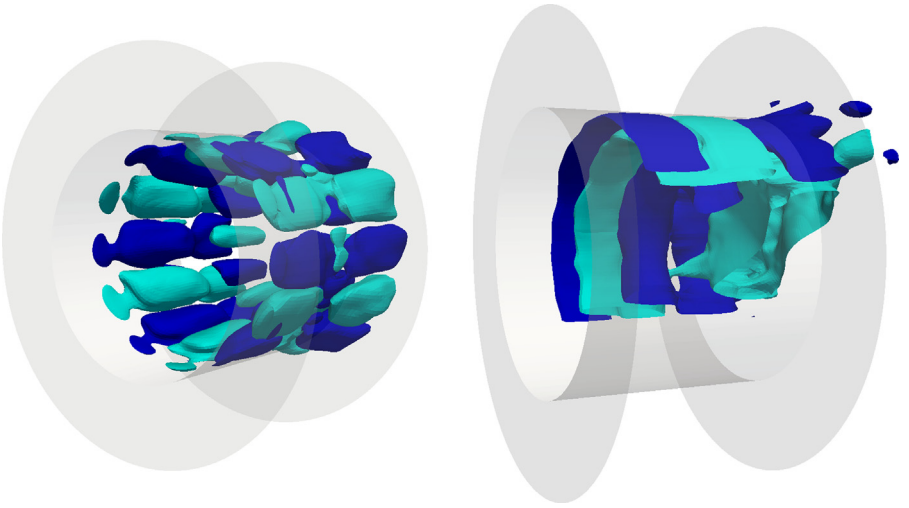

Fig. 29. Shape of the dynamic modes at St=0.4 (left) and St=0.43 (right). Iso-surfaces of a positive and negative axial component.

source, or a broadband source, e.g. Gaussian or exponential. The received power spectra depend on the choice of correlation function, e.g. Gaussian or volume conserving. The received power spectra simplify in the asymptotic case of large rms phase shift; otherwise, the exact received power spectra consists of an attenuated source spectrum plus a series of scattering broadbands. The latter demonstrate how the acoustic energy in the emitted source spectrum is spread over a wider range of frequencies by propagation through turbulence, leading to spectral broadening in the received spectrum.

Written by L.M.B.C. Campos: luis.campos@ist.utl.pt and F.S.R.P. Cunha, IST Lisbon, Portugal.

7.3. LES of acoustic-flow interaction at an orifice plate

The interaction between incoming plane waves and the flow through a thick orifice plate, placed in a circular or square duct, is studied with large eddy simulations (LES) and dynamic mode decomposition (DMD) [43]. DMD is a method for finding significant frequencies in a flow field and their corresponding flow structures [44]. This enables the coupling of important flow phenomena to the acoustic scattering at different frequencies. First, the scattering matrix [45] is computed, to study the reflection and transmission of incoming waves as a function of frequency. The results show a strong amplification of acoustic energy at a Strouhal number of St=0.43 (based on the orifice thickness and the jet velocity), in the circular duct case. DMD is performed on the velocity for both cases, without external excitations. The resulting DMD spectra show that the circular duct case has two peaks in the considered frequency range, while the square duct case only has one peak above the considered range. One of these peaks corresponds to the frequency where amplification of acoustic energy was observed, St=0.43, while the other one is at a slightly lower frequency, St=0.4. Studying the shape of the modes (Fig. 29) it is clear that the amplification of acoustic energy occurs at a frequency where the jet has an axisymmetric instability, while the peak at St=0.4 corresponds to an azimuthal instability that does not interact with incoming plane waves.

Written by: E. Alenius: ealenius@kth.se, Competence Centre for Gas Exchange (CCGex), KTH, Sweden.

References

[1] S.R. Koh, M. Meinke, W. Schröder, Impact of multi-species gas injection on trailing-edge noise, *Computers and Fluids* 75 (2013) 72–85.
[2] C. Bogey, O. Marsden, C. Bailly, Large-eddy simulation of the flow and acoustic fields of a Reynolds number 1e5 subsonic jet with tripped exit boundary layers, *Physics of Fluids* 23 (3) (2011) 035104. (1-20).
[3] C. Bogey, O. Marsden, C. Bailly, On the spectra of nozzle-exit velocity disturbances in initially nominally turbulent jets, *Physics of Fluids* 23 (9) (2011) 091702. (1-4).
[4] K.B.M.Q. Zaman, Effect of the initial condition on subsonic jet noise, *AIAA Journal* 23 (9) (1985) 1370–1373.
[5] C. Bogey, O. Marsden an, C. Bailly, Influence of initial turbulence level on the flow and sound fields of a subsonic jet at a diameter-based Reynolds number of 10e5, *Journal of Fluid Mechanics* 701 (2012) 352–385.
[6] C. Bogey, O. Marsden, C. Bailly, Effects of moderate Reynolds numbers on subsonic round jets with highly disturbed nozzle-exit boundary layers, *Physics of Fluids* 24 (10) (2012) 105107. (1-24).
[7] S. Grizzi, R. Camussi, Wavelet analysis of near-field pressure fluctuations generated by a subsonic jet, *Journal of Fluid Mechanics* 698 (2012) 93–124.
[8] S. Grizzi, R. Camussi, A. Di Marco, Experimental investigation of pressure fluctuations in the near field of subsonic jets at different Mach and Reynolds numbers, *Proceedings of the 18th AIAA/CEAS Aeroacoustics Conference*, AIAA 2012-2257, Colorado Springs, USA, 2012.
[9] A. McAlpine, P.J.G. Schwaller, M.J. Fisher, B.J. Tester, Buzz-saw noise: prediction of the rotor-alone pressure field, *Journal of Sound and Vibration* 331 (2012) 4901–4918.
[10] E.J. Brambley, M. Darau, S.W. Rienstra, The critical layer in linear-shear boundary layers over acoustic linings, *Journal of Fluid Mechanics* 710 (2012) 545–568.
[11] W.F.J. Olsman, M. Lummer, Influence of wind on the noise footprint of a helicopter landing. *Proceedings of the 38th European Rotorcraft Forum*, Amsterdam, The Netherlands, 2012.

[12] M. Gennaretti, C. Testa, G. Bernardini, Frequency-domain method for discrete frequency noise prediction of rotors in arbitrary steady motion, *Journal of Sound and Vibration* 331 (2012).
[13] M. Gennaretti, C. Testa, G. Bernardini, A. Anobile, An analytical-numerical aerodynamic formulation for efficient aeroacoustics analysis of rotorcraft, *Proceedings of Internoise 2012/ASME NCAD meeting*. New York City, NY, August 2012.
[14] R. Schnell, J. Yin, C. Voss, E. Nicke, Assessment and optimization of the aerodynamic and acoustic characteristics of a counter rotating open rotor, *ASME Journal of Turbomachinery* 134 (2012). (061016-15).
[15] R. Schnell, J. Yin, S. Funke, H. Siller, Aerodynamic and basic acoustic optimization of a counter open rotor with experimental verification, *Proceedings of the 18th AIAA/CEAS Aeroacoustics Conference*, AIAA 12-1276913, Colorado Springs, June 2012.
[16] I. Lepot, R. Schnell, G. Delattre, Aero-mechanical optimization of a contra-rotating open rotor and assessment of its aerodynamic and acoustic characteristics, *Proceedings of the Institution of Mechanical Engineers, Part A: Journal of Power and Energy* 225 (7) (2011) 850–863.
[17] V. Fleury, R. Davy, Beamforming-based noise level measurements in hard-wall closed-section wind tunnels, *Proceedings of the 18th AIAA/CEAS Aeroacoustics Conference*, AIAA paper 2012-2226, Colorado Springs, CO, USA, 2012.
[18] H. Parisot-Dupuis, F. Simon, E. Piot, Aeroacoustic sources localization by means of nearfield acoustic holography adapted to wind tunnel conditions, *Proceedings of InterNoise 2011*, Osaka, September 2011.
[19] H. Parisot-Dupuis, F. Simon, E. Piot, Nearfield acoustic holography in wind tunnel by means of velocity LDV measurements, *Proceedings of Acoustics 2012*, Nantes, April 2012.
[20] H. Parisot-Dupuis, *Application de l'holographie acoustique de champ proche en soufflerie par mesures LDV*, PhD Thesis University of Toulouse, ISAE, Toulouse, France, 2012.
[21] T. Padois, C. Prax, V. Valeau, D. Marx, Experimental localization of an acoustic sound source in a wind-tunnel flow by using a numerical time-reversal technique, *Journal of the Acoustical Society of America* 132 (2012) 2397.
[22] E. Piot, J. Primus, F. Simon, Liner impedance eduction technique based on velocity fields, *Proceedings of the 18th AIAA/CEAS Aeroacoustics Conference*, No. 2012-2198, AIAA, 2012.
[23] J. Primus, E. Piotm, F. Simon, An adjoint-based method for liner impedance eduction: validation and numerical investigation, *Journal of Sound and Vibration* 332 (2013) 58–75.
[24] S. Redonnet, E. Manoha, P. Sagaut, Numerical simulation of propagation of small perturbations interacting with flows and solid bodies, *Proceedings of the 7th CEAS/AIAA Aeroacoustics Conference*, AIAA 2001-2223, Maastricht, The Netherlands, 2001.
[25] S. Redonnet, G. Desquesnes, E. Manoha, C. Parzani, Numerical study of acoustic installation effects with a CAA method, *AIAA Journal* 48 (5) (2010).
[26] S. Redonnet, Y. Druon, Computational Aeroacoustics of realistic co-axial engines, *AIAA Journal* 50 (5) (2012).
[27] G. Cunha, *Optimization of a computational aeroacoustics methodology based on the weak coupling of unsteady aerodynamic and acoustic propagation approaches*, PhD Thesis, University of Tolouse, Tolouse, France, 2012.
[28] G. Cunha, S. Redonnet, On the signal degradation induced by the interpolation and the sampling rate reduction in aeroacoustics hybrid methods, *International Journal for Numerical Methods in Fluids* 71 (7) (2013) 910–929.
[29] C.K.W Tam, J.C. Webb, Dispersion-relation-preserving finite difference schemes for computational acoustics, *Journal of Computational Physics* 107 (8) (1993) 262–281.
[30] C. Bogey, C. Bailly, A family of low dispersive and low dissipative explicit schemes for flow and noise computations, *Journal of Computational Physics* 194 (1) (2004) 194–214.
[31] S. Redonnet, G. Cunha, Towards a robust and accurate CFD-CAA coupling procedure for hybrid methods in aeroacoustics – Part 2: on the application of the CFD-CAA surface weak coupling methodology to realistic aircraft noise problems, *Proceedings of the 18th AIAA/CEAS Aeroacoustics Conference*, AIAA 2012-2191, Colorado Springs, USA, 2012.
[32] K. Kucukcoskun, J. Christophe, C. Schram, M. Tournour, Broadband scattering of the turbulence-interaction noise of a stationary airfoil: experimental validation of a semi-analytical model, *International Journal of Aeroacoustics* 12 (1–2) (2013) 58–104.
[33] K. Kucukcoskun, J. Christophe, C. Schram, M. Tournour, Free and scattered field predictions of the broadband noise generated by a low-speed axial fan, *Noise Control Engineering Journal* 61 (2) (2013).
[34] C. Spehr, H. Hennings, H. Buchholz, M. Bouhaj, S. Haxter, A. Hebler, In-flight sound measurements: a first overview, *Proceedings of the 18th AIAA/CEAS Aeroacoustics Conference*, AIAA-2012-2208, Colorado Springs, CO, USA, 2012.
[35] S. Haxter, C. Spehr, Two-dimensional evaluation of turbulent boundary layer pressure fluctuations at cruise flight conditions, *Proceedings of the 18th AIAA/CEAS Aeroacoustics Conference*, AIAA-2012-2139, Colorado Springs, CO, USA, 2012.
[36] N. Hu, H. Buchholz, M. Herr, C. Spehr, S. Haxter, Beitrag verschiedener Strömungsgeräuschquellen zum Flugzeugkabinenlärm, *Proceedings of Deutsche Gesellschaft für Akustik e.V. (DEGA)*, Vol. 38, Jahrestagung für Akustik DAGA 2012, Darmstadt, Germany, 2012.
[37] N. Hu, H. Buchholz, M. Herr, C. Spehr, S. Haxter, Contributions of different aeroacoustic sources to aircraft cabin noise, *Proceedings of the 19th AIAA/CEAS Aeroacoustics Conference*, Berlin, Germany, 2013.
[38] E. Ciappi, F. Magionesi, S. De Rosa, F. Franco, Analysis of the scaling laws for the turbulence driving panel responses, *Journal of Fluids and Structures* (2012).
[39] A. Di Marco, M. Bernardini, S. Pirozzoli, R. Camussi, Multi-variate statistics of the wall pressure field beneath supersonic turbulent boundary layers, *Proceedings of the 18th AIAA/CEAS Aeroacoustics Conference*, AIAA-2012-2053, Colorado Springs, USA, 2012.
[40] C. Asensio, G. Moschioni, M. Ruiz, M. Tarabini, M. Recuero, Methodology and implementation of a thrust reverse noise detection system for airports, *Transportation research Part D* (2013).
[41] C. Asensio, *Aportaciones a los sistemas de discriminación de Fuentes sonoras en la medida de ruido en aeropuertos*, Universidad Politécnica de Madrid, Madrid, Spain, 2012.
[42] L.M.B.C. Campos, F.S.R.P. Cunha, On the power spectra of sound transmitted through turbulence, *International Journal of Aeroacoustics* 3–4 (2012) 475–520.
[43] E. Alenius, LES of acoustic-flow interaction at an orifice plate, *Proceedings of the 18th AIAA/CEAS Aeroacoustics Conference*, AIAA-2012-2064, Colorado Springs, USA, 2012.
[44] P. Schmidt, Dynamic mode decomposition of numerical and experimental data, *Journal of Fluid Mechanics* 656 (1) (2010) 5–28.
[45] R. Glav, M. Åbom, A general formalism for analysing acoustic 2-port networks, *Journal of Sound and Vibration* 202 (5) (1997) 739–747.